



Post-earthquake Behavior of Steel Moment Resisting Frames with Connections Modified by Introducing Reduced Beam Section (RBS)

Kazem Shakeri¹ · Vahid Akrami¹ · Saeed Moradpour¹ · Saeed Khedmati¹

Received: 17 June 2023 / Accepted: 23 March 2024 / Published online: 4 April 2024
© Korean Society of Steel Construction 2024

Abstract

The beam-to-column connections are the most vulnerable locations in steel Moment Resisting Frames (MRFs) subjected to seismic loading. The cyclic deterioration of these structural elements during the earthquakes may cause their failure under subsequent earthquakes. This paper evaluates the post-earthquake behavior of steel moment resisting frames with Welded Unreinforced Flange (WUF) connections modified by introducing Reduced Beam Section (RBS) to improve their seismic behavior. In this regard, investigations were carried out on the connection and structure scales. At the connection scale, a T-shaped beam-to-column connection was modeled numerically and analyzed under several two-phase consecutive cyclic loading in which the maximum displacement amplitude of the first loading phase was varying. Results of this part were used to investigate the effect of multiple loading on the behavior of conventional and modified moment connections and provide data on the range of ultimate rotation capacity for the studied connections. At the structural scale, steel MRFs with WUF and modified RBS connections were compared by performing Incremental Dynamic Analysis (IDA) and extracting fragility curves. Based on the results, it can be concluded that the seismic collapse capacity of the frame with modified connections subjected to consecutive earthquake is considerably higher than that of the conventional MRF.

Keywords Moment resisting frame (MRF) · Reduced beam section (RBS) · Finite element modeling (FEM) · Cyclic loading · Repeated loading · Damage index

Abbreviations

d	Depth of beam in inches	M	Connection moment
$d\delta$	Displacement increment at the end of the beam	M_c	Connection capping moment capacity
$d\varepsilon^p$	Incremental equivalent plastic strain	M_r	Connection residual moment capacity
$d\varepsilon_{ij}^p$	Incremental deviatoric plastic strain tensor	M_y	Connection yield moment capacity
k_e	Elastic stiffness of the panel zone	P	Applied total load at the end of the beam
k_p	Post yield stiffness of the panel zone	S_a	Spectral acceleration
DI_{cyclic}	CVGM damage index	T	Stress triaxiality
E	Modulus of elasticity	T_1	First vibration mode period
		V_p	Full plastic shear resistance of the panel zone
		V_y	Shear yield strength of the panel zone
		α	Ratio defining strain hardening of the panel zone
		γ_y	Yield distortion of the panel zone
		γ_p	Plastic distortion of the panel zone
		ε	Acceptable error
		ε_1	Equivalent plastic strain at the beginning of tensile or compressive excursion
		ε_2	Equivalent plastic strain at the end of tensile or compressive excursion
		ε^p	Equivalent plastic strain

✉ Vahid Akrami
v.akrami@uma.ac.ir

Kazem Shakeri
shakeri@uma.ac.ir

Saeed Moradpour
saeid.moradpour@student.uma.ac.ir

Saeed Khedmati
s.khedmati@uma.ac.ir

¹ Faculty of Engineering, University of Mohaghegh Ardabili, Ardabil, Iran

ϵ_c^p	Equivalent plastic strain at the end of compressive excursion
$\eta_{monotonic}$	Void growth capacity
θ	Connection rotation
θ_p	Connection pre-capping rotation capacity
θ_{pc}	Connection post-capping rotation capacity
θ_u	Connection ultimate rotation capacity
θ_y	Connection rotation at M_y
λ	Material damageability coefficient
ν	Poisson ratio
σ_e	Effective Von-Mises stress
σ_m	Mean stress
σ_u	Ultimate strength
σ_y	Yield stress
Δ	Interstory drift ratio
ΔS_a	Spectral acceleration increment
Δ_{target}	Interstory drift ratio experienced at first record
Λ	Cyclic deterioration parameter

1 Introduction

Moment Resisting Frames (MRFs) are one of the most popular lateral load resisting systems used worldwide for many years. The conventional welded beam-to-column connections used in these structural systems have a fundamental problem which is the brittle failure in connection welds and heat affected zones. This type of brittle failure was observed in the 1994 Northridge earthquake and has been reported in many studies (FEMA-355e, 2000).

Earthquakes may cause damage to structures in different ways; some structures may be undamaged, some may face complete failure, but at the same time, others may have suffered near-severe damage that can be restored with some retrofitting measures. Several studies have been conducted on the effect of these damages on the seismic performance of structures exposed to a second seismic event (Ghaderi & Gholizadeh, 2021; Loulelis et al., 2012; Parekar & Datta, 2023; Ruiz-García & Negrete-Manriquez, 2011; Torfehnejad & Sensoy, 2021). The results of these studies indicate that the occurrence of multiple earthquake events increases structural demands compared to the single earthquake events (Shakeri et al., 2021).

Without adequate seismic improvements or strengthening measures following an initial earthquake, structures may perform poorly in subsequent ground motions. One of the approaches proposed to modify steel MRFs is improving their connection by strengthening, including the use of gusset plates or flange plates (Kiakojouri et al., 2022; Tartaglia et al., 2022a, b). The other approach is to make a weakened area away from the connections e.g. cutting a part of the flange in the beam known as Reduce Beam Section (RBS). In this regard, Meng et al. (2020) used RBS connections

to improve the anti-collapse performance of steel moment frames. Wang et al. (2021) studied the impact resistance of steel moment frames, comparing the effects of different strengthening methods and showed that the retrofitted beam-column connections exhibit improved ductility and energy dissipation. Bahirai and Gerami (2021) conducted an experimental and numerical investigation on the seismic behavior of steel moment connections rehabilitated by asymmetrically weakening in the beam web. It was concluded that the area reduction of the beam would make the connection prone to out-of-plane buckling (Bahirai & Gerami, 2019). Tabar et al. (2022) used reduced web section (RWS) as well as RBS to retrofit the steel moment connections. Also, a similar study is conducted by Sivandi-Pour (2019).

As a general conclusion of previous studies, it can be said that using retrofitted connections can reduce the risk of severe structural damage and significant economic losses. Many researchers have studied various connections and proposed new approaches for their seismic improvement. However, the post-earthquake in-service modification of frame connections and its effects on the seismic behavior of the frame under subsequent earthquakes have not received much attention. In this regard, the current study investigates the post-earthquake behavior of steel MRFs with connections modified by introducing RBS in the frame beams.

A comparison was made between three types of connections: a traditional Welded Unreinforced Flange (WUF) connection that remained WUF after primary earthquake, a WUF connection that was modified by introducing RBS for aftershock; and an RBS connection that remained RBS after the main shock. For this purpose two kinds of analyses were carried out: The first set of analyses were at connection scale. A detailed Finite Element (FE) model was provided for both WUF and RBS connections, and analyzed under several two-phase consecutive cyclic loading in which the maximum displacement amplitude of the first loading phase was varying. The second set of analyses were at frame scale. A four-story two-bay structure was modeled numerically and analyzed under shock-aftershock event using nonlinear Incremental Dynamic Analysis (IDA). The key parameters, assumptions, modeling techniques, and obtained results are discussed in the following sections.

2 Connection-Scale Assessment

Before evaluating the seismic behavior of steel moment frames with conventional and RBS connections, a series of preliminary analyses were carried out at the connection scale, to provide data on the range of ultimate rotation capacity for the studied connections. In addition, the effect of multiple loading on the behavior of conventional and modified connections was investigated.

2.1 Geometry of Models

Two types of moment connections namely conventional moment connection and RBS connection were modeled and analyzed numerically. The studied models were in the form of T-shaped connections obtained from connecting half of the beam and half of the columns of the upper and lower floors. The length of the half-beam and each half-column was assumed to be 2400 mm and 1500 mm, respectively. In accordance with the tests conducted by Shinde et al. (2003), Beam and column sections were assumed to be $H500 \times 200 \times 10 \times 12$ and $H414 \times 405 \times 18 \times 28$ (height \times width \times web thickness \times flange thickness), respectively. It was done to validate the finite element models with the laboratory data. For RBS connection the dimensions of

the cut (i.e., the horizontal distance from face of the column flange to start of the cut, length of the cut and its depth) was calculated as per ANSI/AISC358 (2016). The general configuration of the connection and details of conventional WUF and RBS connections can be seen in Fig. 1a and b, respectively.

2.2 Finite Element Modeling

Nonlinear finite-element software, Abaqus was used to model and analyze the connections (DS Simulia Corp, 2014). Four-noded shell elements with reduced integration (S4R) were used for meshing of the models. A mesh sensitivity analysis was conducted to select the mesh size in different parts of the model. As shown in Fig. 1c, smaller

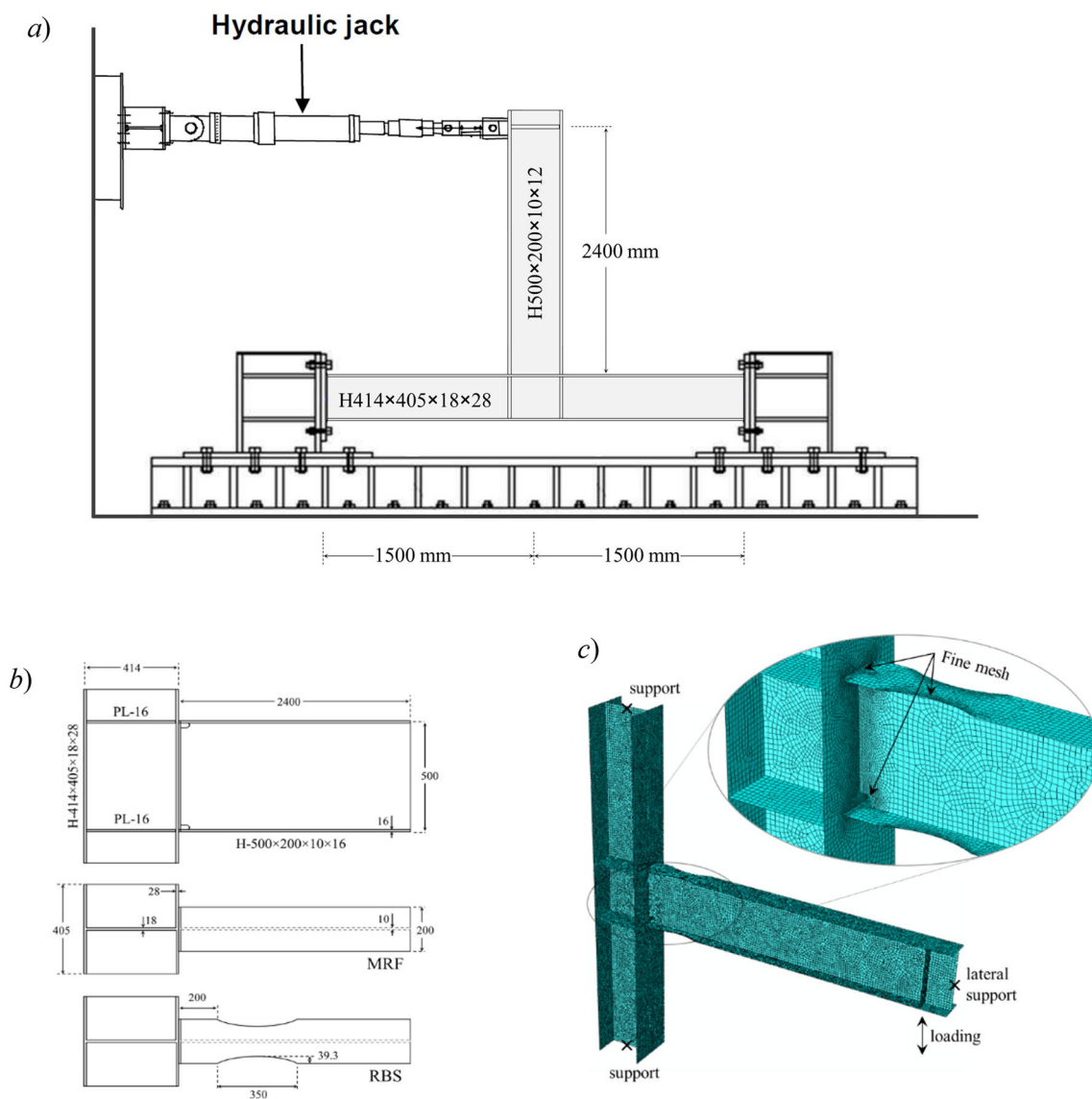


Fig. 1 Modeling details; **a** model configuration; **b** geometry of studied connections; **c** meshing

mesh size was used around the connection welds and RBS region to meet the characteristic length required by fatigue model. Two first buckling mode shapes of the models were used to perturb the intact model and obtain the imperfect model for the cyclic analysis. The nodes located at the top and bottom of the column were constrained to two corresponding reference points, at which the displacement constraints simulating the supports were applied. It is worthy to note that in the modified connection, the RBS parts were cut from the top and bottom flanges of the WUF connection before the onset of second loading phase.

The numerical models included nonlinear material properties and large displacement effects. An associated flow rule with Von-Mises yield surface was used to model the material plasticity. Hardening of the material was defined using a combined isotropic-kinematic model. The mechanical properties of the steel material as reported by Shinde et al. (2003) are summarized in Table 1. According to the table, the steel material used to fabricate the connections and weld them can be categorized as Q345 or its equivalent, SN490B steel.

2.3 Model Validation

The accuracy of models must be ensured before performing the analysis. For this purpose, all characteristics of the studied models including the geometry of the connection, beam and column sections, material properties, etc. were selected according to the tests conducted by Shinde et al. (2003). The connection was modeled and analyzed using the cyclic loading protocol reported in the reference study. Comparing the cycle behavior of the numerical model with the test hysteretic diagram (given in Fig. 2), a good agreement was observed. Furthermore, the buckled shape of the numerical model closely resembled the tested connection, confirming the model’s accuracy.

2.4 Loading Protocol

Two types of loading protocols were used to study the numerical models introduced in the previous sub-sections:

- Single-phase loading: The load history recommended in ANSI/AISC341 (2016) was used for cyclic analysis of

Table 1 Material properties (Liao & Wang, 2010; Shinde et al., 2003; Zhou et al., 2012)

Material	E (GPa)	ν	σ_y (MPa)	σ_u (MPa)	Elongation (%)	$\eta_{monotonic}$	λ
Beam flange steel	206	0.3	323	510	21.6	2.50	0.15
Beam web steel	203	0.3	348	516	19.4		
Column flange steel	214	0.3	374	518	26.9		
Column web steel	205	0.3	352	509	21.6		
Weld	206	0.3	392	513	20.0	2.52	0.20

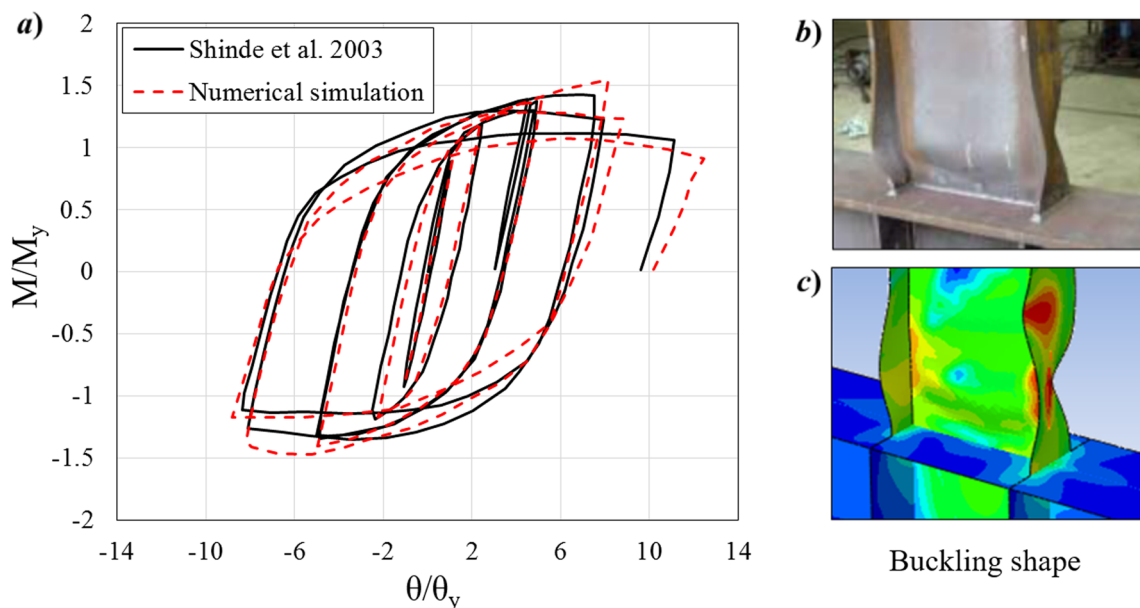


Fig. 2 Verification of numerical models; **a** comparison of hysteretic behavior; **b, c** comparison of buckling shape

the models subjected to single-phase loading. Loading was applied as the displacement at the end of the beam. The adopted loading protocol is plotted in Fig. 3a.

- Consecutive loading: For consecutive loading, six different displacement histories were used, each consisting of two loading phases. The load history recommended in ANSI/AISC341 (2016) was used for both phases, unless the maximum displacement amplitude of the first loading phase was changing. Figure 3b displays the six consecutive loading protocols used in the analyses.

2.5 Evaluation Under Single-Phase Loading

In this section, cyclic load–displacement curves obtained from the analysis of WUF and RBS connections under a single-phase loading are presented and compared. Figure 4a displays these curves for both WUF and RBS connections. According to the figure, for both connections the force–displacement diagram is linear up to approximately 0.01 rad drift ratio and then the curve enters the plastic region. The hysteresis loops are stable up to 0.04 rad drift ratio after which the reduction of stiffness and resistance is evident. Comparing the curves for WUF and RBS connections, it

can be seen that the maximum bearing capacity of the RBS connection is 18% lower than that of the WUF connection.

Figure 5 displays distribution of von-mises stresses at different drift ratios for both WUF and RBS connections. According to the figure, the occurrence of local buckling in the plastic region of the beam has started at the drift ratio of 0.04 and 0.03 radians for WUF and RBS connections, respectively. This shows that the RBS connection is more susceptible to local buckling compared to the WUF connection. As the loading amplitude increases, the local buckling in the vicinity of connection intensifies, and the load–displacement diagram experience further decrease in strength and stiffness (see Fig. 4). It can be expected that the permanent deformations caused in this stage will cause degradation of hysteresis loops under the second phase loading.

2.6 Evaluation Under Two-Phase Loading

This section presents the results of numerical models analyzed under two-phase loading. Three connection types were studied: (a) traditional Welded Unreinforced Flange (WUF) connection remaining WUF after the first phase, (b) WUF connection modified with RBS for the second phase, and (c) RBS connection remaining RBS after the

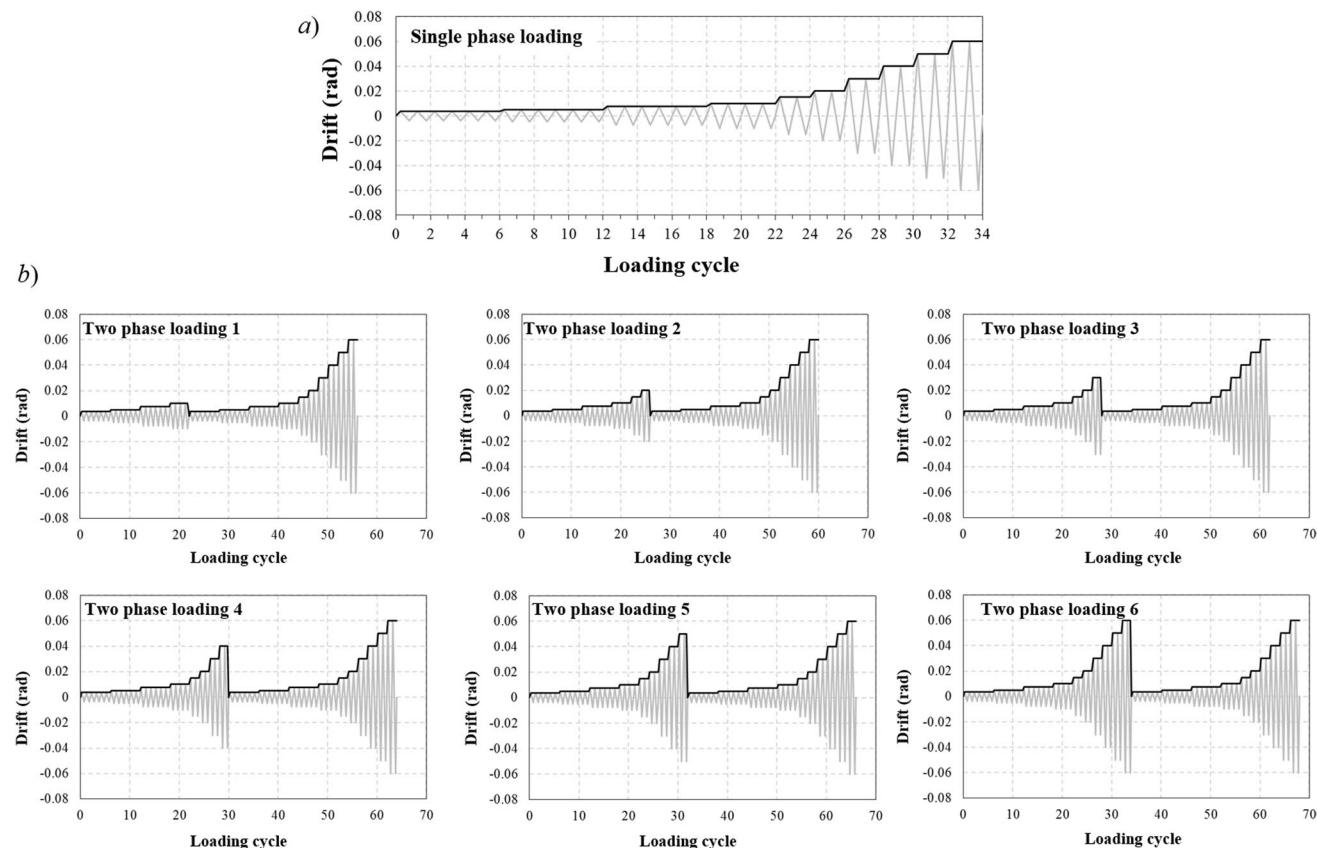


Fig. 3 Cyclic loading protocol; **a** single-phase loading; **b** two-phase loading

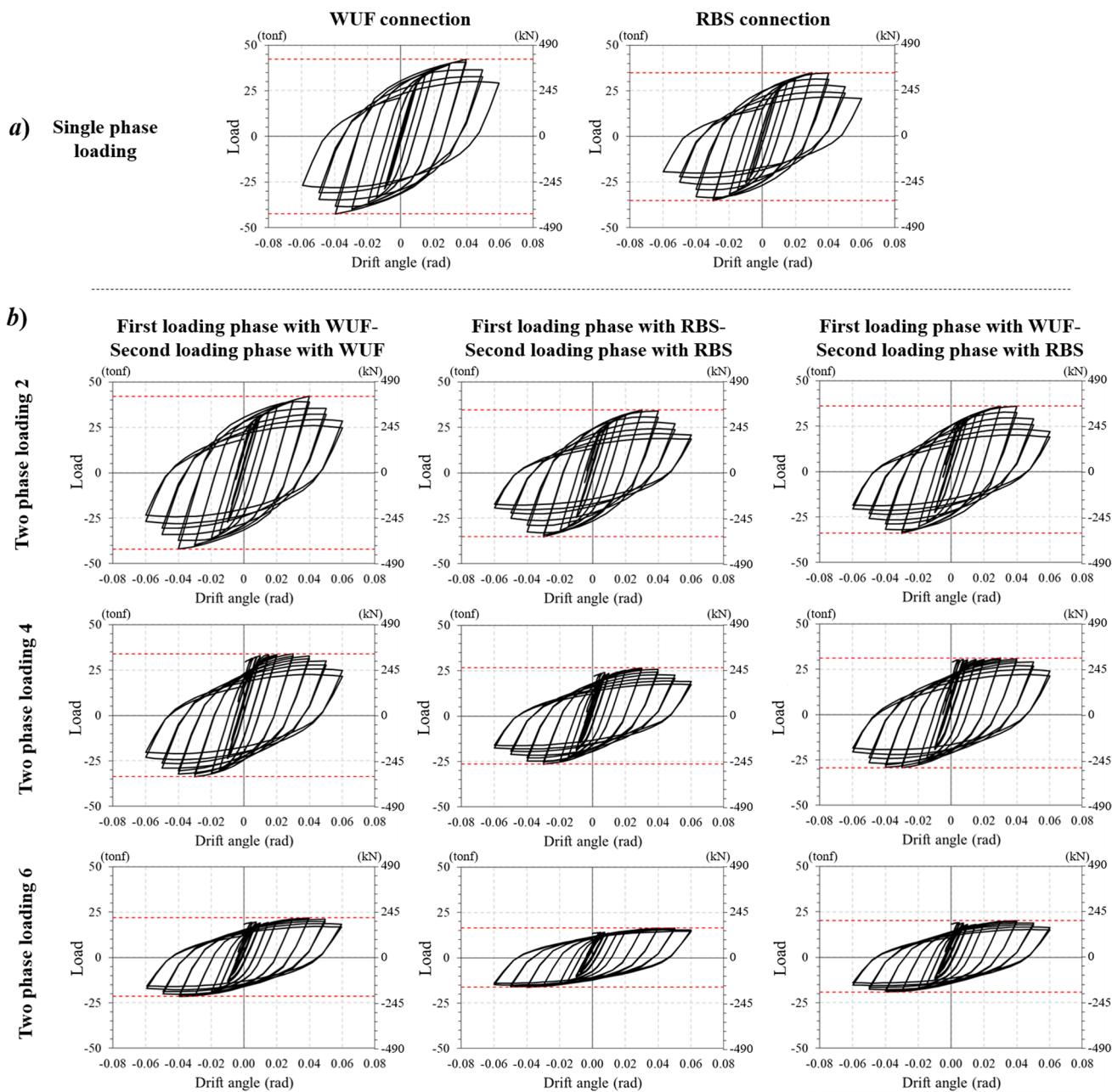


Fig. 4 Load–displacement curves under; a single-phase; and b two-phase loadings

first phase. The effect of primary loading intensity on the connection behavior during the second phase was examined by changing the maximum displacement amplitude of the first phase from 0.01 to 0.06 radians (Fig. 3). Figure 4b shows the cyclic load–displacement behavior of these connections during the second phase. Each column represents a connection type. The curves presented in each row correspond to a primary loading with a specific intensity (not all graphs are presented for brevity). As shown in the figure, for an initial loading with a maximum drift of less than 0.04 radians, the connection behavior is almost the

same under both single-phase and consecutive loadings. However, as the amplitude of the first loading increases to 0.04 radians or more, the loss of stiffness and strength can be seen in the hysteresis loops of the second phase loading. For the initial loading with a maximum drift of 0.06 radians, the maximum connection strength decreases to approximately 50%. In addition to ultimate strength, the dissipated hysteretic energy is often used as a measure of performance for structural components subjected to cyclic loading. This quantity is defined as the area enclosed within the hysteresis loops of the connection, $\int P.d\delta$, in

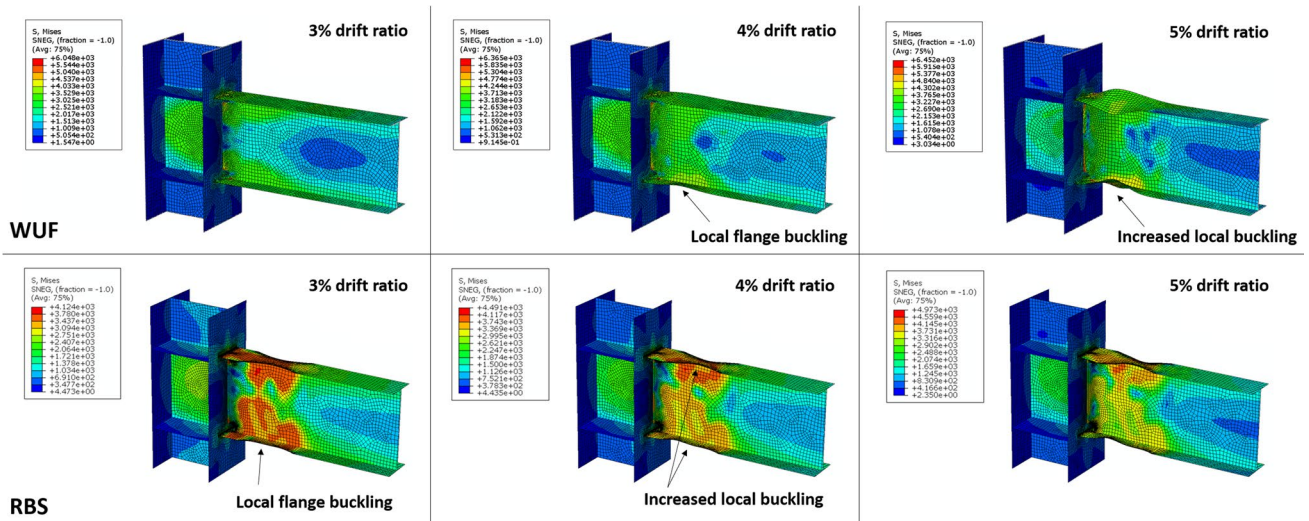


Fig. 5 Distribution of von-mises stresses at different drift ratios

which P and $d\delta$ are the applied total load and displacement increment at the end of the beam. Figure 6a and b illustrate the ultimate bearing capacity and energy dissipation of the studied connections normalized using the corresponding values at single-phase loading. The horizontal axis represents the maximum displacement amplitude of the first loading phase. According to these graphs, the modified connection exhibits the least reduction in bearing capacity and energy dissipation compared to other connections.

Generally, the fracture under cyclic loads such as those induced by earthquakes can be categorized into Ultra Low Cycle Fatigue (ULCF) condition (Zhou et al., 2012). This condition is generally defined by fracture initiation due to a few cycles (e.g. less than 20) of large plastic strains that are usually several times the yield strain (Kanvinde & Deierlein, 2007). The accumulated equivalent plastic strain (PEEQ) in critical elements of the model serves as a measure of damage and indicates vulnerability to ULCF. This parameter, defined using the below equation, can be used as

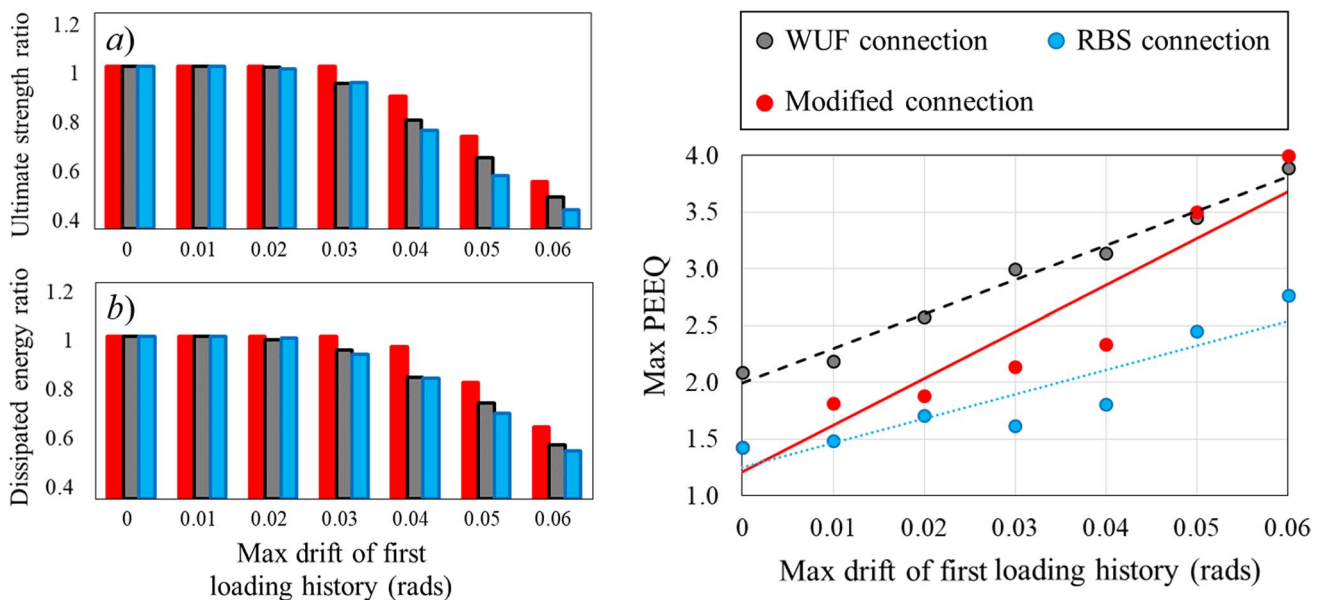


Fig. 6 Comparing of results under two-phase loading; a ultimate bearing capacity; b energy dissipation; c Max PEEQ with respect to pre-load level

a behavioral indicator to compare the analyzed connections (Myers et al., 2009):

$$\varepsilon^p = \int d\varepsilon^p = \int \sqrt{2/3 d\varepsilon_{ij}^p \cdot d\varepsilon_{ij}^p} \quad (1)$$

In this equation, $d\varepsilon^p$, is the incremental equivalent plastic strain, and $d\varepsilon_{ij}^p$ is the incremental deviatoric plastic strain tensor. Figure 6c compares the maximum equivalent plastic strain during the second phase of analysis for WUF, RBS, and modified connections subjected to different loading scenarios.

According to the figure, for the two-phase loading with an empty first phase (analogous to single-phase loading), there is a substantial difference between the maximum PEEQ values of the two models at the end of the analysis. As the maximum displacement amplitude of the first loading phase increases, the maximum value of PEEQ increases for all models. However, for two-phase loading where the maximum displacement amplitude of the first loading phase is less than 0.04 radians, the state of the maximum PEEQ in the modified connection is similar to that of the RBS connection. In contrast, when the maximum displacement amplitude of the first loading phase is more than 0.04 radians, the state of the maximum PEEQ in the modified connection is similar to that of the WUF connection. Accordingly, it can be concluded that modifying the existing WUF connections by introducing RBS can only be effective if the connection has not experienced rotations of more than 0.04 radians. Otherwise, the plastic hinge formed in the vicinity of the WUF connection will be degraded to such an extent that the plastic hinge under the second loading phase will form again in this region even if the connection is modified by introducing RBS.

2.7 Further Investigation

According to the results obtained in the previous section, it was observed that the use of the modified connection is effective only when the initial connection has experienced a maximum plastic rotation less than a certain value. This threshold value corresponds to the state after which the beam plastic hinge experiences extensive damage and loses its stiffness and strength. For a more detailed examination of this threshold value in WUF and RBS connections, the damage index defined by Cyclic Void Growth Model (CVGM) was studied in the finite element models. For this purpose, a Python code was developed to retrieve the stress and strain histories at each element of the model and calculate the CVGM damage index at each time step. Based on the assumptions of CVGM, the damage index due to cyclic loading in ductile metals can be expressed as follows (Kanvinde & Deierlein, 2007; Myers et al., 2009):

$$DI_{cyclic} = \frac{\sum_{tensile} \int_{\varepsilon_1}^{\varepsilon_2} \exp(|1.5T|) d\varepsilon^p - \sum_{compression} \int_{\varepsilon_1}^{\varepsilon_2} \exp(|1.5T|) d\varepsilon^p}{\exp(-\lambda \varepsilon_c^p) \cdot \eta_{monotonic}} \quad (2)$$

In which, T , is the stress triaxiality ($T = \sigma_m / \sigma_e$), σ_m , is the mean stress, and σ_e , is the effective Von-Mises stress. Also, λ , is the material dependent damageability coefficient, ε_c^p the equivalent plastic strain determined at reversal points from a negative to positive triaxiality and $\eta_{monotonic}$ is the void growth capacity for monotonic tensile loading. The values of $\eta_{monotonic}$ and λ for the adopted steel material are reported in Table 1. The first term in the numerator of Eq. (2) evaluates the cumulative void growth over all tensile excursions (i.e. positive triaxiality) while the second term calculates the cumulative void shrinkage over compressive excursions (i.e. negative triaxiality). Thus, the damage index fluctuates during the tensile and compressive excursions. The denominator of Eq. (2) shows the void growth capacity, which decreases continuously during successive loading cycles. The magnitude of triaxiality and equivalent plastic strain governs the rate of the increase of CVGM damage index. For parts of the model with high triaxiality and plastic strains, this quantity increases more quickly. Fracture initiation under ULCF is justified when the CVGM damage index reaches to unity (Kanvinde & Deierlein, 2007; Myers et al., 2009).

Based on the stress and strain histories, the CVGM damage index was calculated for each element at each time step during the analysis of both models. Variation of CVGM damage index during the analysis for the most critical element (the first element at which the damage index reaches unity) on the studied connections is plotted in Fig. 7. According to the figure, it can be seen that the onset of failure in the most critical element of the WUF and RBS connections has occurred at a drift ratio of 0.03 and 0.06 radians, respectively. The rapid increase and the larger variation range of the CVGM damage index in the MRF connection was due to the higher triaxiality and equivalent plastic strain at the end of its beam. As the RBS connection had more uniform stress and strain distributions, the growth rate and range of the CVGM damage index was lower for this model. In general, it can be seen that although the ultimate capacity and the drift ratio corresponding to the local buckling for RBS connection is less than that of WUF connection, its energy dissipation capability will be more than that of WUF connection because its ultimate deformation capacity is higher. This actually reflects the "strong connection-weak beam" philosophy, which protects the connection against the concentration of stress and strain demands.

According to Table 9–7.2 of ASCE/SEI-41 (2017) the ultimate rotation capacity for WUF and RBS connections can be predicted from the following equations:

$$\theta_u = 0.043 - 0.0006 \times d(\text{WUF}) \quad (3)$$

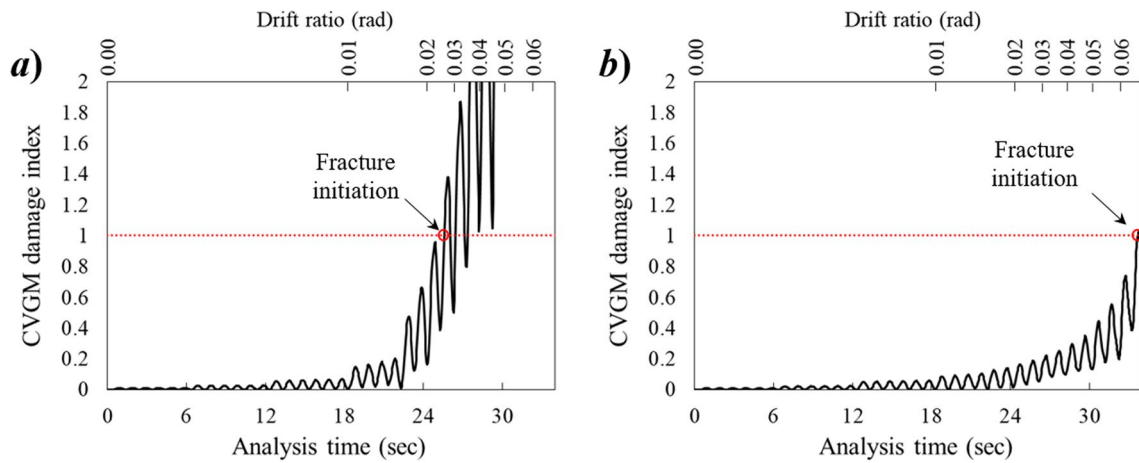


Fig. 7 CVGM failure index history for the most critical element on the; **a** MRF connection; **b** RBS connection

$$\theta_u = 0.070 - 0.0003 \times d(\text{RBS}) \tag{4}$$

In which the parameter *d* is the depth of beam in inches. According to these equations, the ultimate rotation capacities for the studied WUF and RBS connections can be calculated as 0.0312 and 0.0641 radians. According to Fig. 7, the fracture initiation in MRF and RBS models is justified during the first loading cycle to 0.03 radians and the second loading cycle at 0.06 radians, respectively, which is in good agreement with the values obtained from above equations.

3 Frame-Scale Assessment

In this section, the behavior of steel moment frames with WUF and modified connections is compared by performing incremental dynamic analysis and extracting fragility curves. The results obtained from the analyses conducted

at the connection scale have been used in the modeling and analysis of frames in this section.

3.1 Geometry of Model

The four-story office building studied by Lignos (2008) was used for the investigations conducted in the frame scale. The plan and elevation views of this building are shown in Fig. 8a and b. According to Lignos (2008), the total seismic weight on the floors and the roof was assumed to be 4671 kN and 5338 kN, respectively. The building was assumed to be located in Los Angeles on soil type D. The maximum considered earthquake (MCE) spectral response acceleration at short periods and at 1 s period was assumed to be 1.5 g and 0.9 g, respectively. The EW moment resisting frame was selected for investigation. According to Fig. 8, the studied frame had two bays with a span of 9.1 m. The story height was 4.6 m for the bottom story, and 3.7 m for all other stories. The frame was designed assuming A992 Grade 50 steel

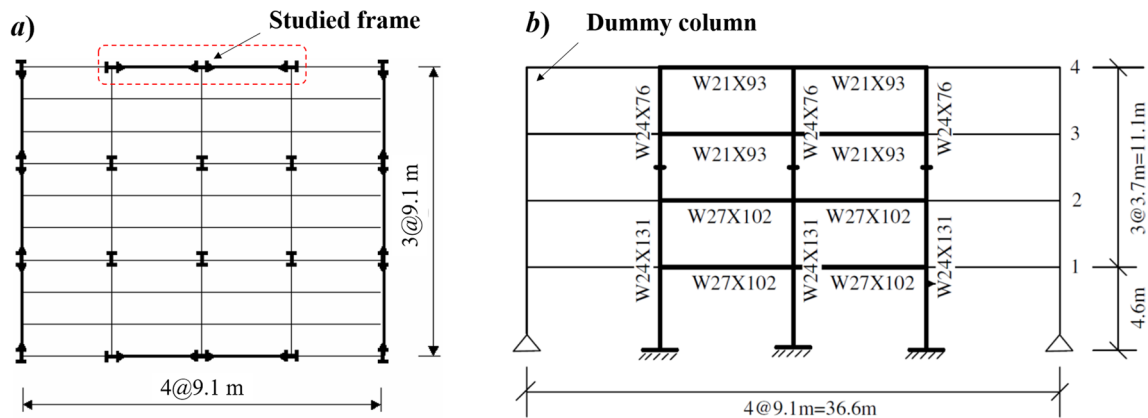


Fig. 8 Plan and side view of the studied frame

for all beam and column elements. The section profiles for beams and columns are shown in Fig. 8b. Two fictitious bays were considered on both sides of the frame to account for the destabilizing effects caused by the gravity loads of the interior frames.

3.2 Finite Element Modeling

OpenSees software was used to model and analyze the frame-scale models. Following the numerical modeling procedure used by Lignos (2008), the nonlinear modeling of the frame was performed based on the lumped plasticity model. The elastic beam-column element was used to model the beams and columns of the frame. The modulus of elasticity and Poisson’s ratio of the steel material were assumed to be 210 GPa and 0.3, respectively. The nonlinear behavior of these elements was assigned to the zero-length rotational springs simulating the plastic hinges. The yield and true ultimate strength of the steel material were assumed to be 345 MPa and 500 MPa, respectively. Figure 9 displays details of the modeling for beam-to-column joint region. According to the figure, each beam and column element had two zero-length elements at the beginning and end. Also, the beam elements had two additional springs simulating the reduced section of the beam. For both type of frames with WUF and modified connections, the zero-length elements corresponding to the reduced section were inactive during the first seismic event, to simulate WUF connections. It was done by adding a rigid spring between the rotational degrees

of freedom of the zero-length elements. For the frame with modified connections, those rotational constraints were removed before the second seismic event, to simulate the modification of connections by RBS. For both WUF and modified connections, the cyclic behavior of the rotational springs was modeled using the modified I–K deterioration model (Lignos & Krawinkler, 2011). According to Fig. 9b, this model only represents the moment-rotation behavior of the hinges and does not account for the interaction of internal forces. Considering that the studied model is a low-rise frame with light to medium axial load in the columns, the adoption of this model for frame plastic hinges can be considered reasonable (Lignos, 2008). The parameters of the I-K model such as yield, capping and residual moment strength, M_y , M_c and M_r , pre-capping and post-capping rotation capacity, θ_p and θ_{pc} , cyclic deterioration parameter, Λ , and etc. were determined based on the relationships provided by Lignos and Krawinkler (2011).

The ultimate rotation capacity, θ_u , for WUF and RBS connections were calculated from Eqs. (3) and (4). The beam-column panel zone area was modeled using the parallelogram model developed by Krawinkler and Mohasseb (1987). The cyclic shear-distortion behavior of this model was governed by a trilinear rotational spring located at the upper right corner of the parallelogram as shown in Fig. 9c. The yield shear strength and distortion, V_y and γ_y , the plastic shear strength and distortion, V_p and γ_p , the elastic and plastic stiffness, k_e and k_p , as well as the strain hardening ratio, α , of the panel zone were determined based on the relationships

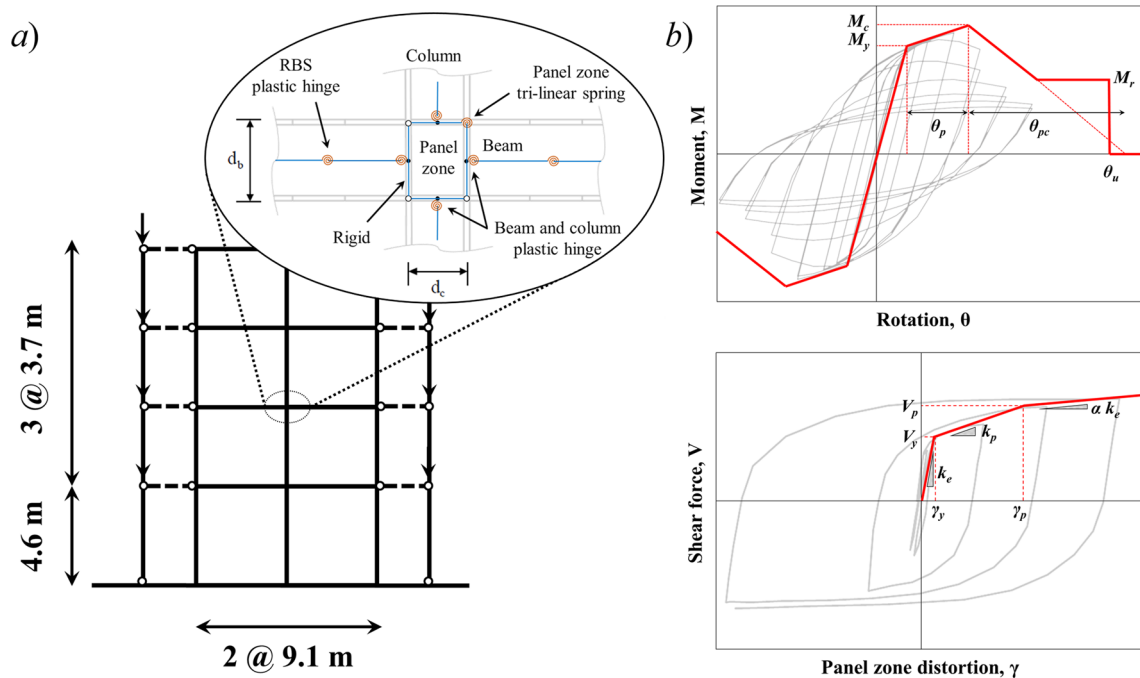


Fig. 9 Details of the modeling for beam-to-column joint in the OpenSees software

provided by Krawinkler and Mohasseb (1987). To consider the P-delta effects of the interior frames, a dummy column was modeled on both sides of the frame using pin-ended rigid beam–column elements. The natural period of the numerical model was calculated to be 1.32 s, which agreed with the value reported by Lignos (2008).

3.3 Ground Motion Records and Scaling

Synthesized acceleration time-histories containing two consecutive earthquake records were used to analyze the numerical models. According to Li et al. (2014), this type of consecutive records can be generated by seeding the recorded ground motions using the repeated or randomized approaches. The repeated seismic sequence that is generated by repeating an earthquake record as both preceding and following seismic events, can be considered as a conservative way to estimate the seismic performance of buildings on the assumption that characteristics of both seismic events are the same (Li et al., 2014). In this research, the FEMA-P695 (2009) far-field ground motion set, comprising 22 ground

motions, was used to synthesize the consecutive records and analyze the frame structures.

For the analysis of structures under consecutive records, first a single-record IDA analysis was performed under each earthquake record. The 5%-damped first-mode spectral acceleration of the models was used for scaling the ground motions (as per FEMA-P695, 2009) based on the flowchart presented in Fig. 10a. For this purpose, the earthquake records were multiplied by a scale factor to match their 5%-damped first-mode spectral acceleration, $S_a(T_1, 5\%)$, with the assumed spectral acceleration, S_a . The numerical model was analyzed under the scaled earthquake records and the corresponding maximum interstory drift ratio was obtained. The assumed spectral acceleration, S_a , was gradually increased using a pre-selected search step, ΔS_a , to force the structure through the entire range of behavior. In case of global dynamic instability of the analyzed model, the search step was halved and the analysis was continued from the last successful step. The IDA curves of these preliminary analyses were used to scale the first ground motion of the consecutive records to the target drift ratio, $\Delta_{target} = 0.04$.

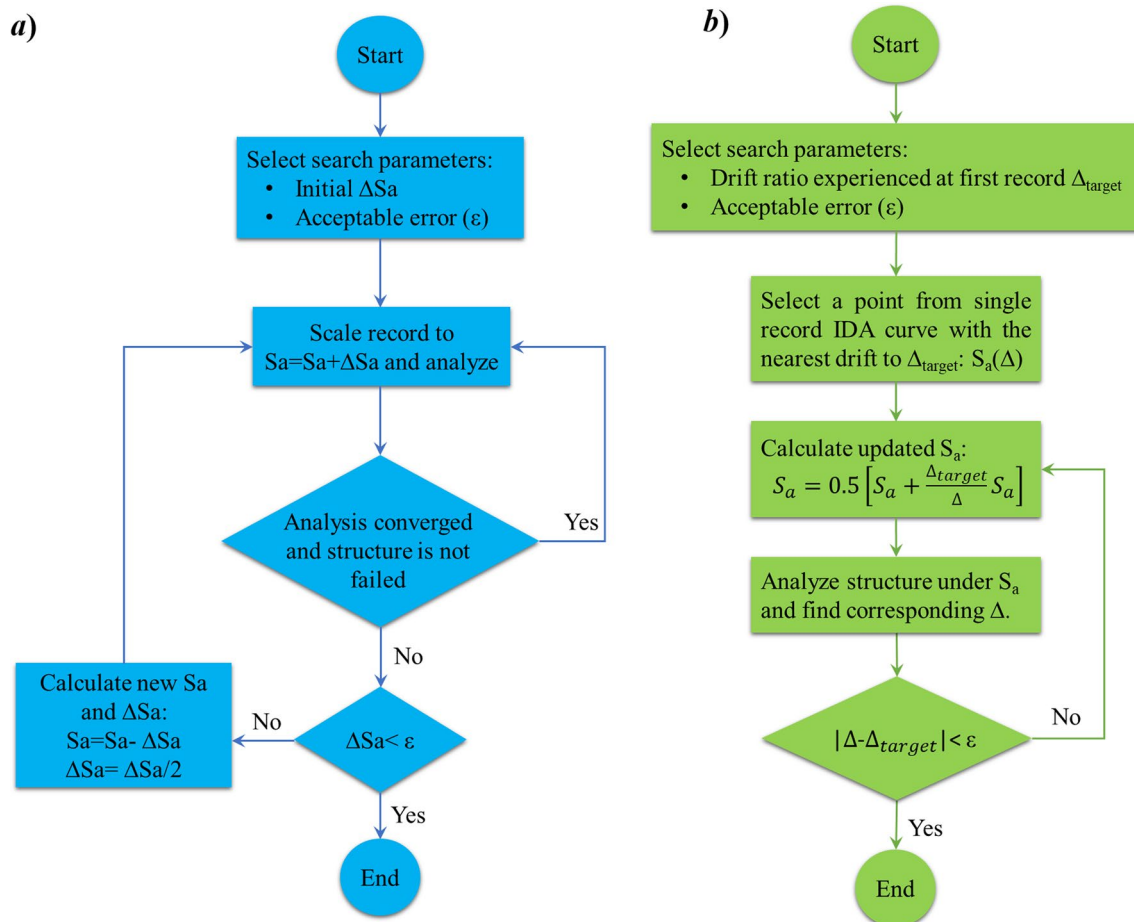


Fig. 10 Analysis flowchart: **a** record scaling for IDA analysis; **b** scaling of the first record to a desired drift ratio

This target drift ratio was selected in such a way as to keep the connection rotations under the first ground motion record below the ultimate rotation capacity, θ_u , for the WUF connection given in Eq. (3). Checking the connection rotations in preliminary IDAs showed that this condition was achieved when the maximum interstory drift ratio was below 0.04 rad. Scaling of the first ground motion record to produce $\Delta_{target} = 0.04$, was done using the flowchart presented in Fig. 10b. The second seismic event was scaled according to the flowchart presented in Fig. 10a to obtain the IDA curve under repeated seismic sequences.

3.4 Results

As a preliminary analysis and in order to have a benchmark to compare the results obtained from IDA under consecutive records, a set of IDAs was conducted to evaluate the seismic collapse capacity under single-record earthquake events. Results of these analyses for frames with WUF and RBS connections are presented in Fig. 11a and b. The grey lines show the curves for individual ground motions while the 16%, 50% and 84% fractiles are shown in black.

According to these graphs, the frame with RBS connections has higher seismic collapse capacity and lower probability of failure under single-record earthquake events. The median collapse capacity for the frame with RBS connections is almost 30% higher than that of the frame with WUF connections. At this spectral acceleration, the collapse probability of the frame with RBS connections is nearly 60% lower than that of the frame with WUF connections. Results of the IDA analysis for frames with WUF and RBS connections subjected to repeated earthquake events are presented in Fig. 11c and d. The frame with modified connections is marked by MC. According to the figure, the frame with modified connections has almost 40% higher median collapse capacity than the original MRF. At this spectral acceleration, the collapse probability of the frame with modified connections is nearly 70% lower than that of the original MRF. Comparison of collapse fragility curves generated by fitting a lognormal distribution to the collapse capacity of the models extracted from Fig. 11a to d is presented in Fig. 12b. As can be seen in the figure, the seismic collapse capacity of the frame with modified connections subjected to repeated earthquake is slightly lower than that of the frame

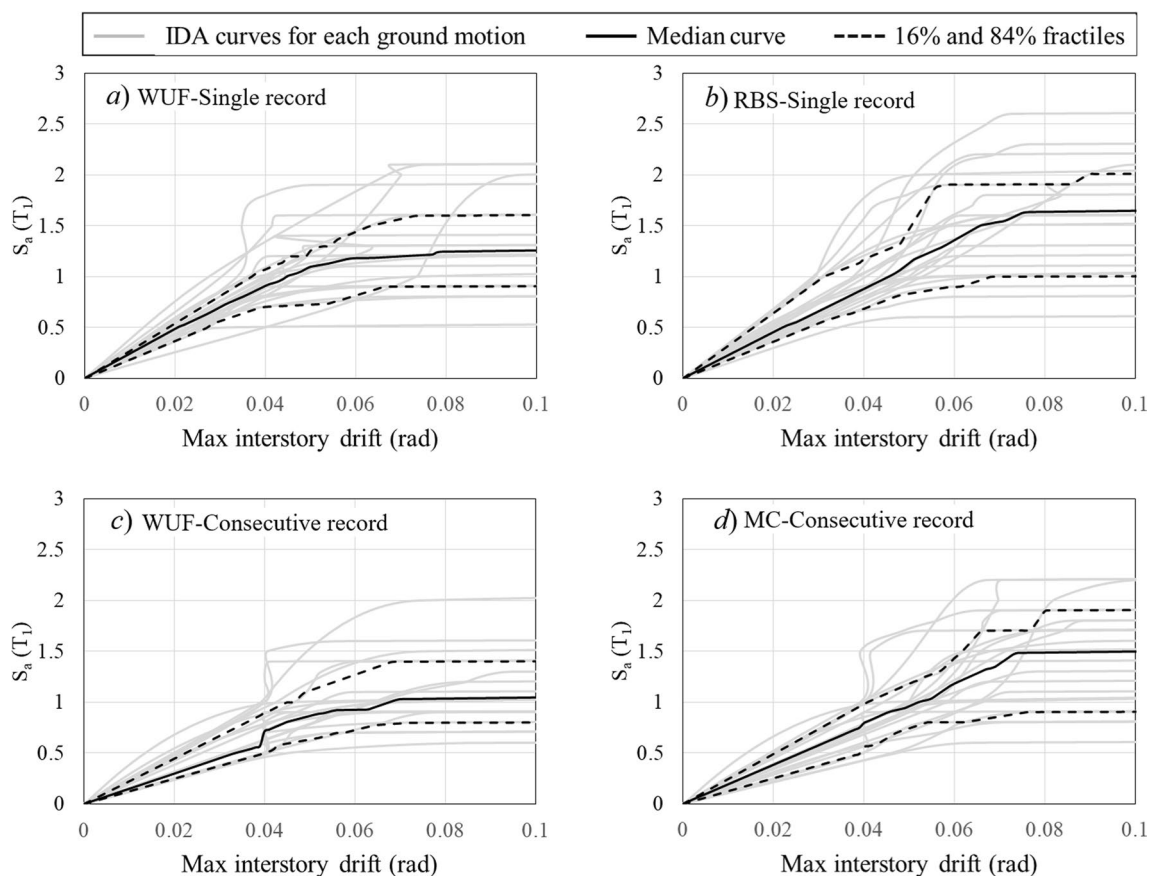


Fig. 11 IDA curves for the frame with **a** WUF connection under single-record events; **b** RBS connection under single-record events; **c** WUF connection under consecutive records; **d** Modified connection under consecutive records

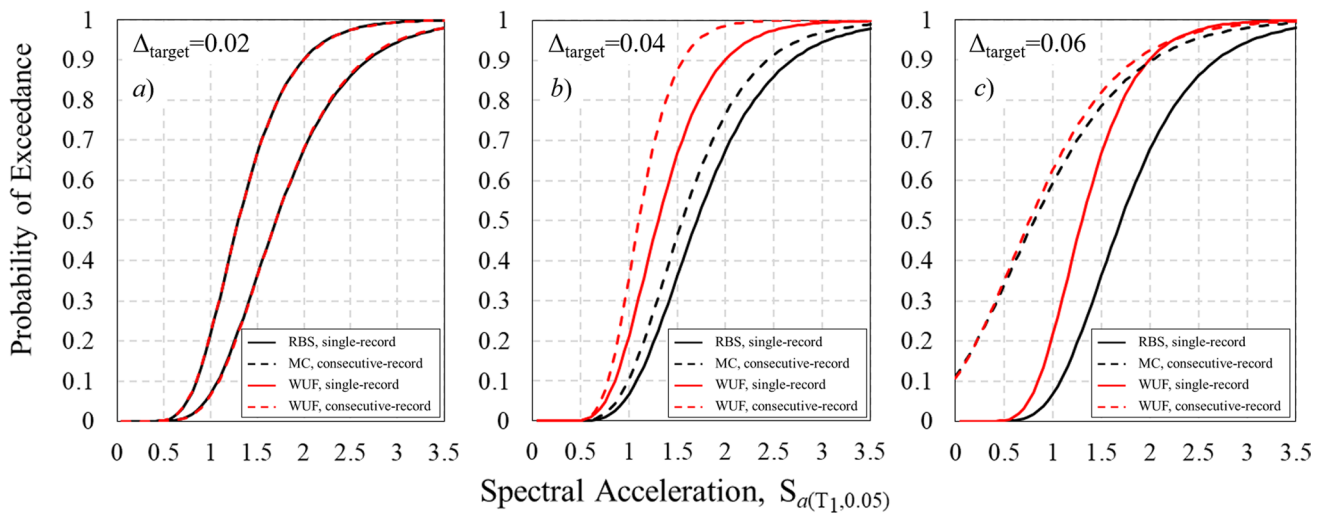


Fig. 12 CP fragility curves for different models at different target drift ratios

with RBS connections subjected to single record event. However, the seismic collapse capacity of this frame is considerably higher that of the conventional MRF subjected to both single- and repeated-record events. This can be due to shifting the location of the plastic hinge from the face of the column flange to the reduced section of the beam.

4 Discussion on Results

In Sect. 2.6, it was concluded that the modification of existing WUF connections by introducing RBS can only be effective if the frame connections have not experienced rotations of more than 0.04 radians. To investigate this hypothesis, models studied in Sect. 3 were re-analyzed using two other values for the target drift ratio of the first ground motion record, i.e. $\Delta_{target} = 0.02$ and 0.06 radians, and collapse fragility curves were plotted in Fig. 12a and c, respectively. As the dataset for the latter case contained zero values, the lognormal distribution was fitted by adding a constant value to all collapse capacities and subtracting the same constant value from the x axis. According to Fig. 12a, it can be seen that for Δ_{target} values less than 0.04 radians, the collapse capacity of the studied frames under single and repeated

earthquakes is quite similar. In this case, the model with modified connections shows 30% higher collapse capacity compared to the original MRF. However, as shown in Fig. 12c, when Δ_{target} is larger than 0.04 radians, both models with original and modified connections show same collapse capacity under consecutive record which is much lower than the capacity of models under single record event. As described in Sect. 2.6, this is because modification of the connections in a frame with severely damaged connections does not affect the location of the active plastic hinges.

Table 2 summarizes the mean total energy dissipated by beam and RBS hinges in the analyzed models. According to the table, in the model with modified connections, the RBS hinges dissipate the main portion of the seismic energy during the second earthquake event. Also, it is evident that for both models with the original and modified connections, as the Δ_{target} increases, the amount of dissipated energy increases in the first earthquake and decreases in the subsequent ground motion. However, the reduction rate of the dissipated energy during the second earthquake event is much higher for $\Delta_{target} = 0.06$ radians. Thus, it can be concluded that for Δ_{target} values greater than 0.04 radians, the participation of RBS hinges in seismic energy dissipation of the frame will decrease greatly.

Table 2 Mean total energy dissipated by beam and RBS hinges (kJ)

Model connections	Hinge type	$\Delta_{target} = 0.02$		$\Delta_{target} = 0.04$		$\Delta_{target} = 0.06$	
		1st record	2nd record	1st record	2nd record	1st record	2nd record
WUF	Beam hinges	5.41	52.49	45.18	37.26	51.31	15.19
	RBS hinges	–	–	–	–	–	–
MC	Beam hinges	5.41	0.04	45.18	0.07	51.31	0.02
	RBS hinges	–	158.19	–	123.85	–	41.16

5 Conclusion

A comparison was made between the use of three types of moment connections: the traditional Welded Unreinforced Flange (WUF) connection remaining as WUF after primary earthquake, the WUF connection modified by introducing RBS for aftershock, and the RBS connection remaining as RBS after the main shock. Investigations were carried out in the connection and structure scales. In the connection scale, a T-shaped beam-to-column connection was modeled numerically and analyzed under single-phase and two-phase cyclic loadings. Results of analyses under single-phase loading showed that the maximum bearing capacity of the RBS connection is 18% lower than that for the WUF connection. However, further studies showed that the onset of failure in the most critical element of the WUF and RBS connections occurs at a drift ratio of 0.03 and 0.06 radians, respectively. Results of analyses under two-phase loading showed that modifying the existing WUF connections by introducing RBS can only be effective if the connection has not experienced extensive damage and has not lost a large amount of its stiffness and strength. Otherwise, the plastic hinge formed in the vicinity of the WUF connection will be degraded to such an extent that the plastic hinge under the second loading phase will form again in this region even if the connection is modified by introducing RBS.

At structure scale, a two-bay four-story steel moment frame with WUF, RBS and modified connections was subjected to a set of repeated earthquakes in which the first record was scaled to produce a target drift ratio equal to 0.04 radians, in the studied frames. The seismic behavior of the frames under the second seismic event was compared in terms of IDA and fragility curves. Results of this part showed that the seismic collapse capacity of the frame with modified connections subjected to repeated earthquake is slightly lower than that of the frame with RBS connections subjected to single record event. However, the seismic collapse capacity of this frame is considerably higher than that of the conventional MRF subjected to both single- and repeated-record events. This can be due to shifting the location of the plastic hinge from the face of the column flange to the reduced section of the beam. Evaluations with larger target drift ratio showed that when the maximum interstory drift ratio during the first ground motion record was larger than 0.04 radians, both models with original and modified connections showed same collapse capacity under consecutive record which was much lower than the capacity of models under single record event. Therefore, it can be said that modifying the existing WUF connections by introducing RBS can be an effective method if the maximum interstory drift ratio experienced

during the preceding ground motions is less than 0.04 radians. Otherwise, it may be necessary to use strengthening methods to repair the yielded parts of the beams.

Statements and Declarations

Conflict of Interest All authors confirm that they have no conflict of interest in publishing this manuscript in the International Journal of Steel Structures.

References

- ANSI/AISC-341. (2016). *Seismic provisions for structural steel building*. American Institute of Steel Construction (AISC).
- ANSI/AISC-358. (2016). *Prequalified connections for special and intermediate steel moment frames for seismic applications*. American Institute of Steel Construction (AISC).
- ASCE/SEI-41. (2017). *Seismic evaluation and retrofit of existing buildings*. American Society of Civil Engineers (ASCE), ISBN: 9780784480816.
- Bahirai, M., & Gerami, M. (2019). Seismic rehabilitation of steel frame connections through asymmetrically weakening the beam. *International Journal of Steel Structures*, 19(4), 1209–1224. <https://doi.org/10.1007/s13296-018-00201-3>
- Bahirai, M., & Gerami, M. (2021). An experimental and numerical investigation on seismic retrofit of steel moment frame connections. *Journal of Earthquake Engineering*, 25(10), 2085–2105. <https://doi.org/10.1080/13632469.2019.1616336>
- DS Simulia Corp. (2014). *ABAQUS analysis user's manual*. Dassault Systemes (DS) Simulia Corp. RI.
- FEMA-355e. (2000). *State of the art report on past performance of steel moment-frame buildings in earthquakes*. SAC Rep., Federal Emergency Management Agency (FEMA).
- FEMA-P695. (2009). *Quantification of building seismic performance factors*. Federal Emergency Management Agency (FEMA).
- Ghaderi, M., & Gholizadeh, S. (2021). Mainshock–aftershock low-cycle fatigue damage evaluation of performance-based optimally designed steel moment frames. *Engineering Structures*, 237, 112207. <https://doi.org/10.1016/j.engstruct.2021.112207>
- Kanvinde, A., & Deierlein, G. (2007). Cyclic void growth model to assess ductile fracture initiation in structural steels due to ultra low cycle fatigue. *Journal of Engineering Mechanics*, 133(6), 701–712. [https://doi.org/10.1061/\(ASCE\)0733-9399\(2007\)133:6\(701\)](https://doi.org/10.1061/(ASCE)0733-9399(2007)133:6(701))
- Kiakojouri, F., De Biagi, V., Chiaia, B., & Sheidaii, M. R. (2022). Strengthening and retrofitting techniques to mitigate progressive collapse: A critical review and future research agenda. *Engineering Structures*, 262, 114274. <https://doi.org/10.1016/j.engstruct.2022.114274>
- Krawinkler, H., & Mohasseb, S. (1987). Effects of panel zone deformations on seismic response. *Journal of Constructional Steel Research*, 8, 233–250. [https://doi.org/10.1016/0143-974X\(87\)90060-5](https://doi.org/10.1016/0143-974X(87)90060-5)
- Li, Y., Song, R., & Van De Lindt, J. W. (2014). Collapse fragility of steel structures subjected to earthquake mainshock–aftershock sequences. *Journal of Structural Engineering*, 140(12), 04014095. [https://doi.org/10.1061/\(ASCE\)ST.1943-541X.0001019](https://doi.org/10.1061/(ASCE)ST.1943-541X.0001019)
- Liao, F. F., & Wang, W. (2010). Parameter calibrations of micro-mechanics-based fracture models of Q345 steel. *Science paper online*, <<http://www.paper.edu.cn/index.php/default/releasepaper/content/201007-457>>. (in Chinese).

- Lignos, D. (2008). *Sidesway collapse of deteriorating structural systems under seismic excitations*. PhD Thesis, Stanford University.
- Lignos, D., & Krawinkler, H. (2011). Deterioration modeling of steel components in support of collapse prediction of steel moment frames under earthquake loading. *Journal of Structural Engineering*, 137(11), 1291–1302. [https://doi.org/10.1061/\(ASCE\)ST.1943-541X.0000376](https://doi.org/10.1061/(ASCE)ST.1943-541X.0000376)
- Loulelis, D., Hatzigeorgiou, G., & Beskos, D. (2012). Moment resisting steel frames under repeated earthquakes. *Earthquake and Structures*, 3(3–4), 231–248. <https://doi.org/10.12989/eas.2012.3.3.231>
- Meng, B., Zhong, W., Hao, J., & Song, X. (2020). Improving anti-collapse performance of steel frame with RBS connection. *Journal of Constructional Steel Research*, 170, 106119. <https://doi.org/10.1016/j.jcsr.2020.106119>
- Myers, A. T., Deierlein, G. G., & Kanvinde, A. M. (2009). *Testing and probabilistic simulation of ductile fracture initiation in structural steel components and weldments*. John A. Blume Earthquake Engineering Center, Technical Report 170. Stanford Digital Repository.
- Parekar, S. D., & Datta, D. (2023). Evaluation of drift demands in vertically irregular steel frames under mainshock–aftershock using equivalent single-degree freedom methodology. *Journal of Vibration Engineering & Technologies*, 11(3), 771–792. <https://doi.org/10.1007/s42417-022-00608-7>
- Ruiz-García, J., & Negrete-Manriquez, J. C. (2011). Evaluation of drift demands in existing steel frames under as-recorded far-field and near-fault mainshock–aftershock seismic sequences. *Engineering Structures*, 33(2), 621–634. <https://doi.org/10.1016/j.engstruct.2010.11.021>
- Shakeri, K., Akrami, V., Shokrgozar, H. R., & Arden, A. (2021). Comparing responses of special and intermediate moment frames under repeated earthquakes. *Proceedings of the Institution of Civil Engineers-Structures and Buildings*, 175(11), 847–864. <https://doi.org/10.1680/jstbu.20.00051>
- Shinde, H., Kurobane, Y., Azuma, K., & Dale, K. (2003). Additional full-scale testing of beam-to-column connections with improvements in welded joints. In *Proceedings of the thirteenth (2003) international offshore and polar engineering conference*, Honolulu, Hawaii, USA.
- Sivandi-Pour, A. (2019). Performance assessment of steel moment connections retrofitted with various reduced section patterns. *Civil and Environmental Engineering Reports*, 29(4). <https://doi.org/10.2478/ceer-2019-0041>
- Tabar, A. M., Alonso-Rodriguez, A., & Tsavdaridis, K. D. (2022). Building retrofit with reduced web (RWS) and beam (RBS) section limited-ductility connections. *Journal of Constructional Steel Research*, 197, 107459. <https://doi.org/10.1016/j.jcsr.2022.107459>
- Tartaglia, R., Milone, A., D’Aniello, M., & Landolfo, R. (2022a). Retrofit of non-code conforming moment resisting beam-to-column joints: A case study. *Journal of Constructional Steel Research*, 189, 107095. <https://doi.org/10.1016/j.jcsr.2021.107095>
- Tartaglia, R., Milone, A., D’Aniello, M., De Martino, A., & Landolfo, R. (2022b). Seismic assessment of beam-to-column joints for a non-conforming MRF existing structure. In *10th international conference on the behaviour of steel structures in seismic areas*, Timisoara, Romania.
- Torfehnejad, M., & Sensoy, S. (2021). Energy absorption and inelasticity distribution mechanisms in steel moment frames affected by mainshock-aftershock sequences. *Structures*, 33, 3550–3569. <https://doi.org/10.1016/j.istruc.2021.06.082>
- Wang, H., Huo, J., Elchalakani, M., Liu, Y., & Zhang, S. (2021). Dynamic performance of retrofitted steel beam-column connections subjected to impact loadings. *Journal of Constructional Steel Research*, 183, 106732. <https://doi.org/10.1016/j.jcsr.2021.106732>
- Zhou, H., Wang, Y., Shi, Y., Xiong, J., & Yang, L. (2012). Extremely low cycle fatigue prediction of steel beam-to-column connection by using a micro-mechanics based fracture model. *International Journal of Fatigue*, 48, 90–100. <https://doi.org/10.1016/j.ijfatigue.2012.10.006>

Publisher's Note Springer Nature remains neutral with regard to jurisdictional claims in published maps and institutional affiliations.

Springer Nature or its licensor (e.g. a society or other partner) holds exclusive rights to this article under a publishing agreement with the author(s) or other rightsholder(s); author self-archiving of the accepted manuscript version of this article is solely governed by the terms of such publishing agreement and applicable law.